Space Systems Design Laboratory

Development of Maneuverable Deep Space Small Satellites

AE 8900 Special Problem Report

Author:
Matthew D. Wilk

Advisor:
Dr. E. Glenn Lightsey

Space Systems Design Laboratory
Daniel Guggenheim School of Aerospace Engineering
Georgia Institute of Technology
May 6th, 2019

Development of Maneuverable Deep Space Small Satellites

Matthew Wilk [*]and Glenn Lightsey [†]

Propulsion systems of some form are required for most CubeSat missions looking to venture beyond Low earth Orbit (LEO). The Lightsey Research Group has been producing additively manufactured satellite thrusters for various missions since 2012 and is experienced in their designing, manufacturing, testing, and operation of such systems. These thrusters traditionally have been printed using stereolithography (SLA) methods, but new metal printing techniques allow for the use of traditional aerospace aluminum alloys. Metal printing of thrusters allows for the combining of satellite structure with propulsion system piping and tanks contained within the satellite. This research examines the design process for a 1U additively manufactured satellite with propulsion designed into the structure, the design and simulation of a new feedback control scheme for angular momentum management, and documents the efforts made towards radiation tolerant electronics. The sum of works contained within are towards the common goal of enabling more beyond LEO CubeSats.

I.   Introduction and Motivation

Small satellites known as CubeSats have been around since the late 1990's and an overwhelming majority have been constrained to low Earth orbit (LEO) applications. CubeSats serve as a way to train young space engineers in the art of designing, manufacturing, and operating a space mission, as well as providing lower-cost test beds for raising the Technology Readiness Level (TRL) of experimental space technologies. CubeSats have their roots in science and acadamia, but in recent years they have shifted into the commercial and government sectors as the aerospace industry begins to recognize CubeSats as a lower-cost option for testing or conducting new missions.

The cost of developing spacecraft and launching them has been prohibitively expensive until recently for entrepreneurs seeking to develop space-based industries. Partially due to this large cost-barrier to entry, the space-based economy has been restricted to military, communication, and scientific domains. However, the advent of CubeSats is encouraging more risk-taking and innovation in the space industry. Startup companies built around small satellites such as Planet Labs and Planetary Resources use these tiny satellites for daily Earth photography and asteroid prospecting.

The majority of CubeSats have reached space by way of ride-sharing on large rockets as secondary payloads. This means that the small satellites have had to reach space and operate in suboptimal orbits due to the restriction of the primary payload selecting the rocket's trajectory. In addition, not every rocket that launches has secondary payloads making the total number of opportunities for CubeSats less. Due to this shortage of launches with secondary payloads, an entire new section of the launch market has developed to launch CubeSats. Companies like FireFly, Rocket Labs, Vector, Virgin Orbit, and others are dedicated solely to the design, manufacture, and launch of smaller vehicles for the express purpose of launching these small satellites. The smaller launch vehicles carry a lower cost to space access than other traditionally used launch vehicles. For instance, the Rocket Lab Electron rocket delivers 150 kg to sun-synchronous orbit for the cost of $4.9 million USD.[1] This more tenable cost and the ability to select the final orbit makes purchasing one of these new small launch vehicles appealing to CubeSat manufacturers.

---

[*]Graduate Student, Guggenheim School of Aerospace Engineering, 270 Ferst Drive, Atlanta, GA. 30313, USA

[†]Professor, Guggenheim School of Aerospace Engineering, 270 Ferst Drive, Atlanta, GA. 30313, USA

American Institute of Aeronautics and Astronautics

The CubeSat industry has blossomed with LEO applications, but scientists and engineers have sought to use CubeSats beyond LEO for gathering more data at a fraction of the cost. Interplanetary space missions are some of the most expensive, and they are also time constrained since launches occur in yearly epochs due to the alignment of planets. For these reasons, scientists and engineers seek ways to maximize the amount of scientific data gathered by these missions without making overly-complicated missions that get canceled and never fly. For example, the Tethering and Ranging mission at the Georgia Institute of Technology (TARGIT) is developed around this idea. Putting a LIDAR on a small satellite that rideshares with a Mars mission can be used to gather terrain data on Mars' moons Phobos and Deimos. These two moons which orbit a high-science target, Mars, have scant data available. Russia has sent three probes total to Phobos, only one of which successfully reached Mars and returned data fron Phobos, whereas Deimos has yet to be examined by any spacecraft.

The age of interplanetary CubeSats is here. On November 26th 2018, the Mars Cube One (MarCO) satellites flew by Mars to send data back to Earth during the Entry, Descent, and Landing phase of the InSight mission. Had these small satellites not been there, scientists and engineers would have had to wait hours to know if InSight had successfully landed on Mars.

MarCO A and B, like most satellites, require the ability to orient themselves in space. Reasons for needing this capability include pointing solar panels for power generation, pointing antennae for communications, and pointing instruments at celestial objects to take measurements. Most small satellites in LEO use either magnetic torque rods or reaction wheels, or a combination to achieve their pointing needs. Magnetic torque rods are electromagnets that when turned on interact with the Earth's magnetic field and spin the spacecraft. Reaction wheels can be very precise with pointing, but are susceptible to angular momentum build-up. Small perturbations and torques in the space environment may be managed with reaction wheels since spinning them will store this momentum in the wheels, thus allowing the body of the spacecraft to remain in the desired orientation. However, reaction wheels are limited by the fact that they can only spin so fast. Once they reach this saturation point, any further torques or perturbations will cause the spacecraft to spin uncontrollably, effectively ending the mission. Magnetic torque rods and reaction wheels are used in tandem on LEO small spacecraft missions with need for precise pointing abilities since the reaction wheel stores momentum and the torque rod may be turned on to slowly dump the momentum from the spacecraft.

As these small satellites are used in more applications beyond LEO, they need to find different ways of unloading momentum from reaction wheels. As satellites move away from the Earth, the magnetic field strength drops off considerably rendering magnetic torque rods useless. Larger satellites use reaction control thrusters with either hypergolic fuels or others like ammonium perchlorate. Propulsion systems thus far on small satellites have been largely undeveloped for a number of reasons ranging from volume constraints inside the satellite, safety issues with pressurized systems, fuel toxicity, and others. However, the Lightsey Research Group (LRG) between the University at Texas Austin and the Georgia Institute of Technology has developed cold gas propulsion systems for five different satellite missions since 2012.[2] These missions have ranged from proximity operations[3],[4] interplanetary[5],[6] and geostationary CubeSat missions.

Cold gas systems provide propulsion without the combustion of any propellants. Instead, all thrust force is generated by opening a valve connecting a gaseous reservoir to the vacuum of space. The pressure of the propellant along with the nozzle geometry and molecular size of propellant determine characteristics like thrust and efficiency. LRG thrusters operate using a two-tank principle. The first tank is filled with a saturated liquid-vapor mixture of the propellant, and the second is an expansion tank known as the plenum where the pressure of the vapor is kept below the saturated liquid-vapor pressure. This expansion tank is used to ensure propellant is in a gaseous phase before exiting the thruster system to avoid rapid density changes in the nozzle, in addition to isolating the main propellant tank from space. If valves were connected straight to the main tank and stuck open, then all of the propellant would vent into space.

Stevenson[7] explains why volumetric efficiency is especially important for CubeSats. CubeSats more often are constrained by volume than by mass limitations, especially since small satellites are frequently able to apply for mass waivers from deployers. However, if there is not enough volume, CubeSat designers will need to increase the unit size of their satellite possibly jeopardizing a launch opportunity or incurring additional cost to the mission. Large chunks of volume in small satellites is generally occupied by items such as batteries

and reaction wheels. In the case of batteries, until power management systems are made even more efficient and battery sizes made smaller for the same energy capacity, power will be a volumetric pain point for many CubeSat missions.

The purpose of this work is to further the study and design of additively manufactured small satellites with integrated propulsion systems. Maneuverable CubeSats allow for the design of formation flying small satellite constellations, and they also allow for deep space missions like the MarCO A and B CubeSats which need propulsion when operating beyond LEO. In fact, both MarCO satellites possessed cold gas propulsion systems onboard similar to the thrusters produced by LRG.[8] In addition, as other missions plan for destinations beyond LEO they too will require some sort of propulsion to keep their reaction wheels from saturating and ending their missions early. Hence there is this great need for the further study of volumetrically efficient cold gas propulsion systems for CubeSats.

II.   Design of an Additively Manufactured Maneuverable Satellite

Previously developed LRG cold gas thrusters have made use of stereolithography (SLA) printed materials to store propellant as a liquid-vapor mixture moved between the plenum and main tank. As additive manufacturing techniques improve, metal printing of designs is now possible with aluminum alloys.[9] Some of the limitations of SLA printed thrusters are that the materials are not always space-safe or low-outgassing, and that some materials may degrade due to radiation damage. What is a further hindrance is the scant literature about the space compatibility of these materials. This means when selecting materials for an SLA printed thruster, the designer has to go through the process of determining what printed materials are capable of surviving the space environment.

There is also the issue of propellant compatibility with SLA printed materials. The propellant used by LRG is the refrigerant HFC-236fa, or R-236fa. This propellant is desired due to its high volumetric impulse[7] and low toxicity,[10] but it does have limitations. To know if it is compatible with SLA printed materials requires lengthy and costly test campaigns, whereas R-236fa is not known to react with metals.[10] Thus using metal printed structures provides a benefit from both an outgassing and propellant compatiblity point of view since most metals are generally space safe and compatible with the propellant of choice. If for any reason a metal printed material is found to be incompatible, there are is a larger list of alternative materials that might be safe as well.

Due to higher strength, metal printed structures allow for thinner tank walls and thus more propellant storage than SLA printed thrusters. Satellite missions are life-limited by propellant unless a critical system fails beforehand, so maximizing propellant load is desired. Metal printed thrusters enables printing thrusters using the satellite's own structure. Stevenson[7] designed a 3U CubeSat named the Satellite Propulsion Unit Demonstrator (SPUD) which is additively manufactured from printed aluminum with a thruster system including pipes, nozzles, and tanks all inside the structure of the satellite. Printing thruster systems into satellite structures allows for less volume used by internal components like fasteners and attachment tabs, so that more volume goes to the thruster propellant tanks. The following work presented examines the design process of a 1U CubeSat version of SPUD to compare the performance capabilities to a traditional SLA printed thruster of approximately the same size. Determining the capabilities of a 1U SPUD system informs mission designers about the capabilities of different sizes of these maneuverable and volume efficient CubeSats.

For the design of this additively manufactured hybrid-satellite-propulsion system, it is desired to design a satellite that could achieve full 6 degrees of freedom in its movement. In order to adhere to as many CubeSat deployer specifications as possible, the CalPoly CubeSat specification[11] was chosen to model the satellite with. However, due to the severe volume limitations present, four of the required eight nozzles were removed so that necessary satellite subsystem components would be able to fit inside the empty volume. This is because the four nozzles in question would have been placed opposite of the remaining four nozzles with piping in the CubeSat rails. However, in the interest of fitting actual CubeSat electronics inside, the nozzles were chosen to be removed.

The result of the design effort is the following 1U CubeSat structure shown in Figure 1 known SPUDnik, a simplified version of SPUD. The structure is printed to the specification's geometries with thruster piping,

American Institute of Aeronautics and Astronautics

tanks, and nozzles all designed into the aluminum structure. The thruster system design itself is very similar to previous Lightsey Research Group cold gas thrusters having a two-tank system, temperature and pressure sensors to monitor propellant state for each tank, propellant filling ports, and a manifold with valves and circuit board to control fluid flow between tanks and nozzles. A large advantage of metal printing is that these pressure and temperature sensors, as well as the fill ports can be threaded directly into the CubeSat structure. This eliminates at least four additional o-ring seals found on other LRG thrusters. Reducing the number of o-ring seals necessary is of large importance because it translates to less paths for propellant to possibly leak out.

Most fastener holes pictured in Figure 1 would be added in post-machining of the structure except for those needed in the thruster system itself. Threading of holes on the structure would also be done as part of post machining to ensure clean threading on the structure. The remainder of the empty volume not dedicated to the thruster is available for the hardware and electrical components needed for a satellite mission. The printed part also has a location on the side opposite the thruster for an end cap to close the structure. An example of a completed maneuverable 1U spacecraft is shown in Figure 2. This assembled satellite has an electrical system with 2 batteries and solar panels, a UHF antenna and transceiver, a flight computer, 2 sun sensors, and approximately 20 millimeters of space between thruster system and board stack for additional components. This assembled spacecraft demonstrates the severe volume constraints present on 1U CubeSats, although it also establishes that such a satellite can function and with a propulsion system included. Most 1U CubeSats are simplistic in their design and operation making this a perfect test satellite for cold gas thruster technology.
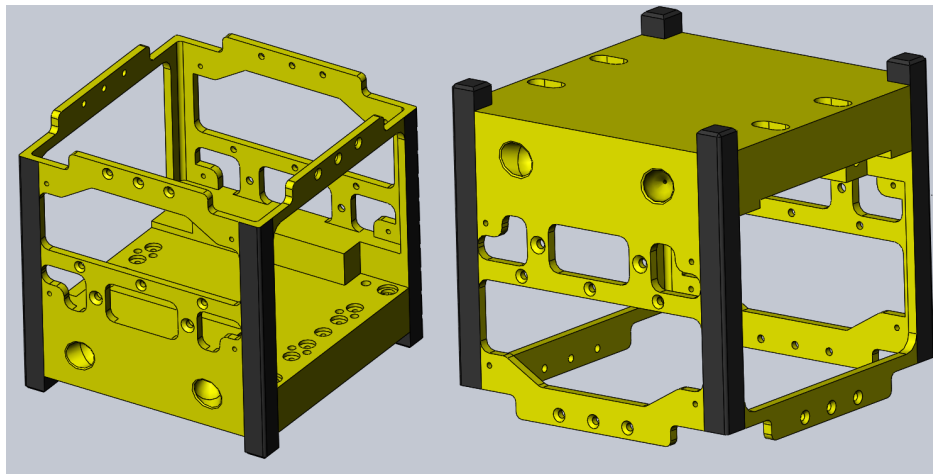

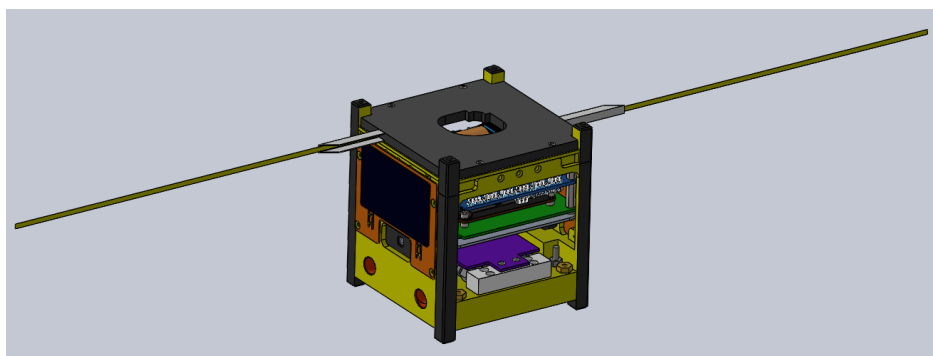Figure 1. Additively Manufactured 1U Structure with Propulsion

Figure 2. Integrated Additively Manufactured CubeSat

Internal views of SPUDnik are shown in Figures 3 and 4. The main tank containing the saturated liquid-

American Institute of Aeronautics and Astronautics

vapor mixture of R-236fa is shown in blue, with the expansion plenum tank containing vapor shown in green. The red features show off the piping and nozzle geometry printed into the structure. The additional 8 holes shown are through holes for bolts to attach the valve manifold to the printed structure. However, a better view of the internals might be shown by the negatives of these internals.
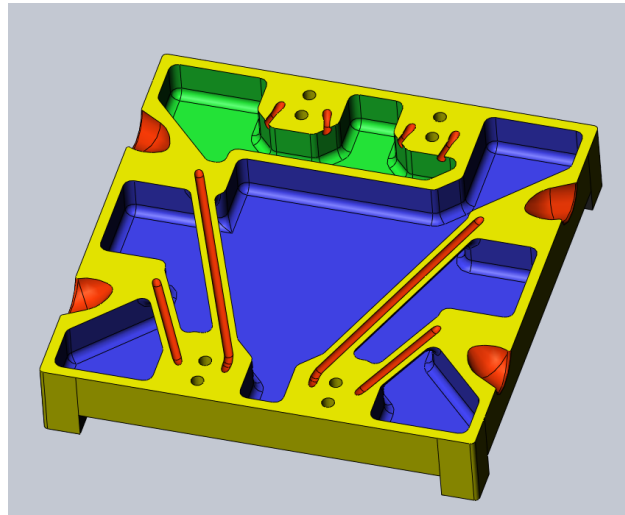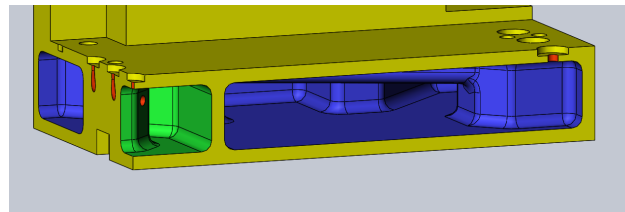

Figure 3. Internals of Structure

Figure 4. Internals Side View

Figures 5 and 6 show the negatives of the printed structure tank. These show the tank volumes in whole as continuous voids for propellant to occupy. These views also give perspective on the tight constraints between the tanks, piping, and nozzles. The internal geometry for the locations of the temperature and pressure sensors is best shown here with additional holes in each tank shown in Figure 5.

Table 1. Comparison of SLA Printed Thruster to Metal Printed Satellite With Thruster

Quantity	SPUDnik	Bevo-2
Overall Volume	300000 mm^3	339400 mm^3
Main Tank Volume	78000 mm^3	90000 mm^3
Plenum Volume	13000 mm^3	6900 mm^3
Propellant	0.098 kg	0.114 kg
Total Impulse	43.2 N-s	50.4 N-s
Main Tank Volume Percentage	0.26	0.27
Number of Nozzles	4	1

$$J = m_{prop}I_{sp}g_0 \tag{1}$$

A comparison of SPUDnik to the original Lightsey Research Group SLA printed thruster for the Bevo-2 mission is shown in Table 1. It is important to note here that the propellant mass for Bevo-2 is calculated
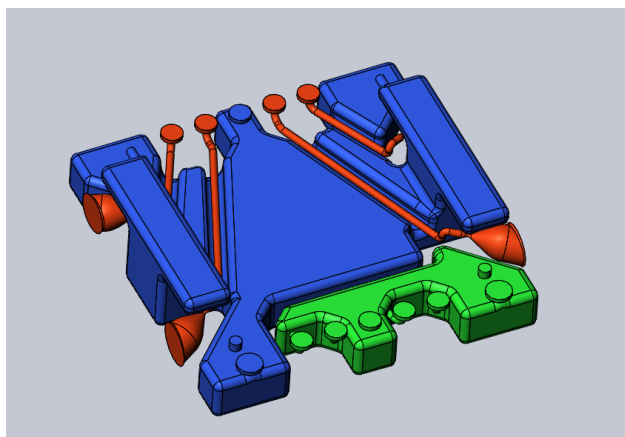
American Institute of Aeronautics and Astronautics
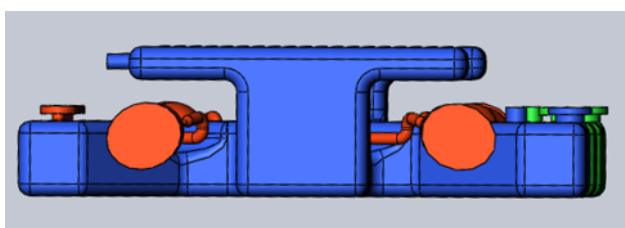
Figure 5. Internals Negative View

Figure 6. Internals Negative Side View

in the same way that it is calculated for SPUDnik as Bevo-2 possibly underestimated their propellant capabilities in their original assesment.[2] The total impulse for both is also calculated according to equation 1 using a specific impulse of 45 seconds.[5] SPUDnik uses this specific impulse because the satellite employs the same nozzle geometry and propellant as the BioSentinel thruster. Calculations for Bevo-2 use the BioSentinel specific impulse because of the uncertainties associated with measuring thrust and impulse with their employed methods.

Table 1 shows at first glance that the Bevo-2 SLA print outperforms SPUDnik in terms of propellant mass and total impulse. However, these are due to the fact Bevo-2 has a larger main tank than SPUDnik. In fact, the overal Bevo-2 allocated volume is approximately 40,000 mm^3 larger than SPUDnik's volume allocation. If even less than half that additional volume allocation went to the main tank of SPUDnik, it would easily outperform Bevo-2. In a smaller volume allocation, SPUDnik has three more nozzles and only 16 grams less propellant than Bevo-2. This makes SPUDnik an obviously more capable thruster in a smaller volume allocation, while nearly matching Bevo-2 in propellant capacity.

Examining the scarfed nozzles printed into the structure shown in more detail by Figure 7, it is easy to see the normal converging-diverging nozzle geometry used on Lightsey Research Group thrusters. However, this view also shows the asymmetric nozzle extension, or scarf, used for this particular set of nozzles. Previous work by Stevenson[7] used protruding blocks for the nozzles so that the nozzle exit plane was coincident with the surface of the satellite. In order to adhere to the CalPoly specification and also maximize the amount of tank volume for propellant, the decision was made to sink the nozzles into the structure and accept any performance losses associated.

Scarfed nozzle geometry requires that the scarf angle β be greater than the Mach angle μ.[12] Due to other limitations like pipe routing and attempting to maximize tank volumes, the nozzles were chosen to have orientations that allow for full angular state control and one linear direction of control for ΔV maneuvers. According to Lilley,[12] the scarf geometry adhering to the Mach angle constraint will not have to deal with

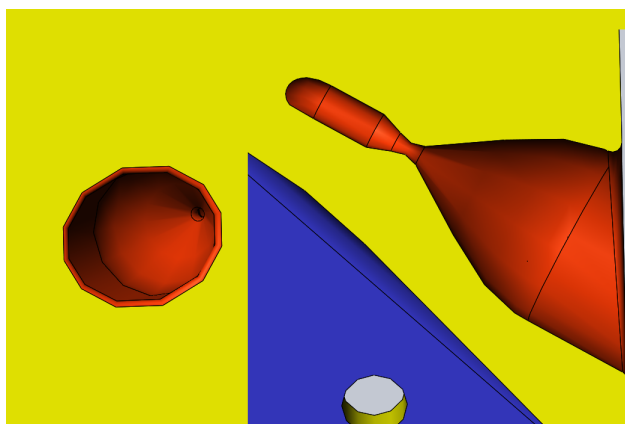American Institute of Aeronautics and Astronautics

Figure 7. Scarfed Nozzle Geometry

downstream flow out of the nozzle interfering with upstream flow. Thus performance impacts are negligible and will not be accounted for in the simulation.

Alternatively, if the design for SPUDnik was changed to a single nozzle ΔV thruster, according to the rocket equation:

$$\Delta V = I_{sp}g_0 ln(\frac{m_0}{m_f}) \tag{2}$$

The thruster would be able to provide approximately 33 m/s of ΔV capability assuming a specific impulse of 45 seconds and satellite mass of 1.33 kg. It is also worthy to note that with the reduction of the number of nozzles from 4 to 1 that more volume could be dedicated to the main tank which means more propellant, meaning more ΔV capability.

III.   Angular Momentum Controller

The current state of LRG thruster controllers involve the use of a very simple schemes. These modes are known colloquially as: 1) dead-reckoning mode and 2) closed-loop mode. These control schemes focus on the necessity for refilling the plenum tank after nozzle firings due to tank pressure driving performance. These modes can be thought of in more simpler terms as a timer based and pressure-comparison based.

Dead-reckoning mode is used in case of emergency that either the plenum or main tank pressure sensors are determined to be having problems. In this mode the refill valve that connects the main tank and plenum is opened for an experimentally determined amount of time after firing for a certain amount of time. This keeps the plenum roughly charged so that the thruster can still work in case of lost sensors. The closed-loop mode currently used checks the pressure between main tank and plenum. Since propellant in the main tank is held as a liquid-vapor mixture and the plenum requires vapor only, the plenum pressure is kept a percentage below the main tank pressure. However, since the thrust and thereby impulse performance of the thruster are driven by plenum pressure only, having a lower threshold limit also ensures that each nozzle firing performs to a standard.

The work presented here is the introduction of a feedback control scheme using both tank pressures and an inertial measurement unit (IMU) for managing the momentum of a deep-space satellite. This controller is motivated primarily for the reason that these systems are used for momentum management, and current thruster systems work only by sending commands of how long to open valves. By introducing another layer of measurements, the thruster processor can determine on its own how long to open valves.

The work presented outlines the process of setting up the problem, identifying the dynamics, developing a thruster performance simulation, and then using results from the performance simulation to develop a Simulink model to model the 1U additively manufactured satellite using a stateflow controller.

American Institute of Aeronautics and Astronautics

A. Problem Setup

The development of a controller is mission and thruster placement dependent. Additively manufactured thrusters are constrained by the volume they are allotted. Because of this, certain nozzle placement configurations may be impossible or need to be modified due to the requirements of the mission. For the development of an angular momentum management system alone, full control is possible through the use of a minimum of 4 nozzles strategically placed and canted. Hence, the 1U additively manufactured satellite thruster system described in the last section is used as a case study for this simulation and controller design.

1. SPUDnik Dynamics

For this problem, one may be tempted to use the Newton-Euler equations of motion to describe the rotational dynamics of the SPUDnik spacecraft. Looking at Table 1 it is clear that the propellant mass represents nearly 10 percent of the overall system mass. Because of this, it is prudent to account for the change in mass, which requires some slight modifications to the Newton-Euler equations as described in the following. Starting at the basic equation that the sum of moments is the inertial frame derivative of the angular momentum:

$$\sum_{i=1}^{N} \vec{\mathbf{M}}_G = {}^{\mathcal{F}}\dot{\vec{\mathbf{H}}}_G = \frac{d}{dt}[\mathbf{I}]\vec{\omega} \tag{3}$$

One will arrive with the task of taking the derivative of the product of the inertia matrix and the angular velocities. Assuming that the axes are body fixed, the derivatives of inertia terms normally go to zero. However, since we are relaxing the assumption that mass is held constant, these inertia derivative terms are non-zero. Thus arriving at the following:

$$\sum_{i=1}^{N} \vec{\mathbf{M}}_G = [\dot{\mathbf{I}}]\vec{\omega} + [\mathbf{I}]\vec{\alpha} + \vec{\omega} \times \vec{\mathbf{H}}_G \tag{4}$$

Where the last term accounts for the rotation of the angular momentum derivative into the inertial frame. In this equation, it is clear that the sum of the moments is not simply equal to the product of inertia and angular acceleration. Since the dynamics of the problem are controlled through the angular acceleration, the equation can be rearranged to solve for it.

$$\vec{\alpha} = [\mathbf{I}]^{-1}\left(\sum_{i=1}^{N} \vec{\mathbf{M}}_G - [\dot{\mathbf{I}}]\vec{\omega} - \vec{\omega} \times \vec{\mathbf{H}}_G\right) \tag{5}$$

Normally, the Newton-Euler equations also make the assumption that the body fixed axes of the object are also the principle axes so that cross-axis inertia terms go to zero. For purposes of this simulation, cross inertia terms are not ignored to keep high fidelity in the simulation.

2. Set up of Controller Design

Since the valves used are isolation valves, they only have binary states instead of analog positions to control flow between the tanks and nozzles. Because of this, controller design is a modified version of previous thruster controllers. The closed-loop mode used previously is still present, but only for the purpose of determining when to ignore commands firing commands. Instead of firing commands being timed sequences as previous thrusters have implemented, this controller design feeds in angular rate data to figure out thrust commands necessary to achieve a desired rotation rate state.

Whether that state is angular rate or angular momentum is dependent on the end user, but for purposes of this controller the controller is for angular momentum. This decision is motivated primarily by the idea that deep space CubeSats will have a thruster system for unloading angular momentum from reaction wheels. By making a controller based around angular momentum management, this paper works towards enabling deep space CubeSat missions using Lightsey Research Group developed technology.

The stateflow diagram of the angular momentum controller is shown as Figure 8. This diagram shows the process of state checking that the controller uses to determine what valves to open. Since the control
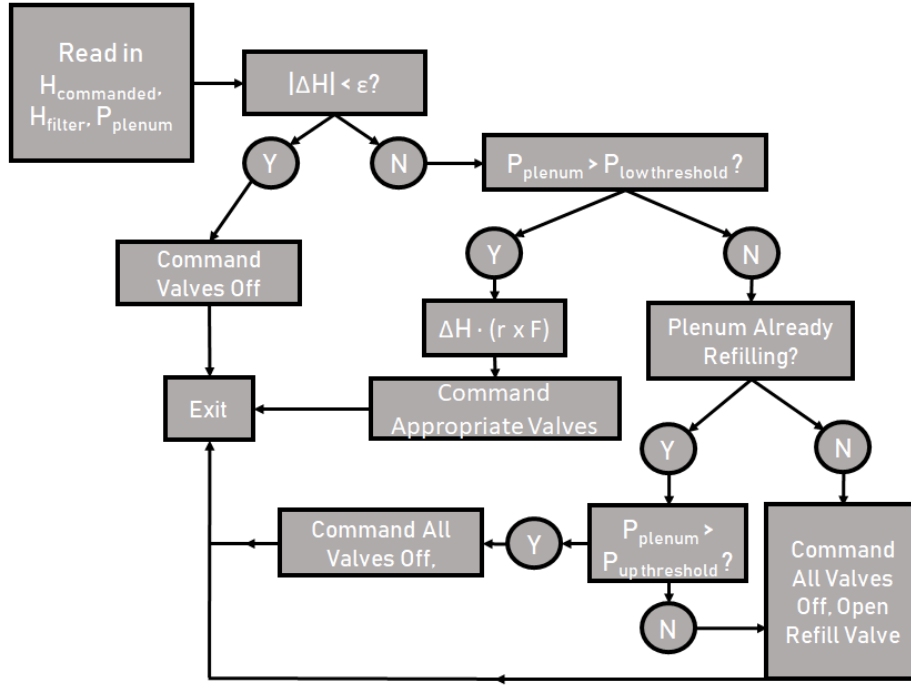
Figure 8. Controller Logic

scheme is bang-bang, the most influence an engineer has over the controller is to set what the upper and lower thresholds are for the controller. The upper and lower thresholds are pressure levels set by the control engineer for regulating pressure levels in the plenum. The plenum can only either have the refill valve or nozzle valves open at a time since opening both refill and nozzle valves at the same time exposes the main tank to the vacuum of space, which can result in the total loss of propellant. Thus, the controller needs to decide when plenum pressure levels have dipped too low before refilling to a pre-determined upper threshold for repeatable performance. It is thought that these thresholds should be percentage values of the pressure in the main tank. However, if the pressure sensor for either tank is noisy or stops working, then this control scheme is useless and the thruster will have to rely on the dead-reckoning mode.

$$\Delta \vec{\mathbf{H}} = \vec{\mathbf{H}}_{filtered} - \vec{\mathbf{H}}_{commanded} \tag{6}$$

The controller calculates the change in angular momentum still needed to meet the command shown in equation 6. The estimated angular momentum is compared to the commanded angular momentum to find the change required.

$$\|\Delta \vec{\mathbf{H}}\| \geq \epsilon \tag{7}$$

Equation 7 shows the logic for determining if any thrust maneuvers need to take place. If the magnitude is greater than some pre-determined tolerance level, then the thruster controller needs to figure out which thrusters to fire. To do this, the controller uses a pre-calculated set of moment arms found by crossing the nozzle exit plane location vectors with thrust unit vectors. The moment arms are dotted with the change in angular momentum vector to determine which nozzles need to fire for the thruster to achieve the command. Moment arms which contribute to driving the norm of change in angular momentum towards zero are chosen.

$$\Delta \vec{\mathbf{H}} \cdot (\vec{r}_{noz,i} \times \hat{\tau}_{noz,i}) \tag{8}$$

It is important to mention that current thruster electronics are limited to firing four valves at any one time. Because of this, more robust controllers need to take this a step further and select the top four dot product values and ignore the rest when it comes to choosing which nozzles to command.

American Institute of Aeronautics and Astronautics

Because this is a cold gas thruster, the vapor filled plenum will deplete as it is exposed to vacuum and thrust is produced. Plenum sizes are rather small compared to main tank volume sizes, and this tradeoff between plenum and main tank sizing is dependent primarily on how often one needs to command the For the refilling logic, the refilling valve between main tank and plenum is opened while all other valves are commanded shut indefinitely. The thruster checks to make sure it is not below a certain threshold akin to previous thrusters. However, this thruster continues to refill until it meets a certain higher second threshold to make sure that it produces sufficient thrust for a certain amount of time unlike previous systems which open for an arbitrary amount of time. If implemented on a real system, it would be prudent to make the refilling steps able to time out in case of emergency where a sensor dies and the computer does not think the plenum is refilling ever. However, for purposes of this design and model this is neglected since the simulated sensors never fail.

B.   Thruster Simulation

To sufficiently model the effects of this thruster and controller on the dynamics of spinning SPUDnik, a model of the thruster itself needed to be developed. For all intents and purposes, flow is modeled as isentropic and the propellant is modeled as a perfect gas. The equation of state for a perfect gas is given as:

$$PV = \frac{m}{MW}\bar{R}T \tag{9}$$

Where P is the pressure in the plenum, V is the volume of the plenum, m is the mass of propellant in the plenum, MW is the molecular weight of the propellant, $\bar{R}$ is the universal gas constant, and T is the temperature of the gas in the plenum.

The metrics of interest for modeling a thruster are: 1) the rate at which mass leaves, 2) the rate of pressure loss in the plenum, 3) the thrust produced, and 4) the specific impulse of the nozzle. The pressure and temperature state of gas in the plenum as well as restrictors in the fluid path will dictate the mass flow rate of propellant out of the plenum and nozzle. Because of this, it is possible to solve for the mass flow rate $\dot{m}$ and then use that value to solve for how other things are changing in time. Mass flow rate is written with the continuity equation which is:

$$\dot{m} = \rho A u \tag{10}$$

Where ρ is the density of the fluid at the point of interest, A is the cross-sectional area of the fluid path, and u is the fluid velocity. Using the perfect gas assumption, density may be rewritten to give the following:

$$\dot{m} = \frac{P}{RT}Au \tag{11}$$

Where R represents the specific gas constant for R-236fa. This means that if flow velocity, flow pressure, and flow temperature can be found at a point in the fluid path, then mass flow rate can be solved. Since this is a cold gas thruster, thrust will change with pressure, which will change with mass flow rate. To find the changing rate of pressure, take a time derivative of equation 9.

$$\frac{d}{dt}(PV) = \frac{d}{dt}\left(\frac{m}{MW}\bar{R}T\right) \tag{12}$$

$$\dot{P}(t) = \dot{m}RT + mR\dot{T} \tag{13}$$

Assuming that the pressure and temperature in plenum are stagnation quantities and assuming that stagnation temperature does not change with time for this analysis, the equation may be simplified to:

$$\dot{P}(t) = \dot{m}RT_0 \tag{14}$$

Thus it is now possible to specify initial plenum conditions and use a numeric integrator to find the state of gas in the plenum over time to see how the thruster performs. The next thing to model though is the actual thruster system itself. The thruster may be modeled by the following flow schematic.

The indicated points are the post-valve conditions denoted by p, the throat flow conditions denoted by t, and the exit flow conditions denoted by e. The valves used are sourced from the Lee company, which uses
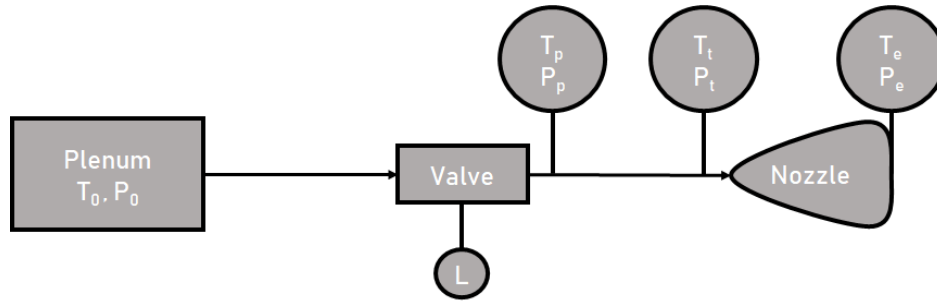
American Institute of Aeronautics and Astronautics

Figure 9. Thruster Flow Model

a proprietary system for measuring flow resistance across their valves called the liquid ohm or Lohms for short. The Lohm rating for the valve is denoted in Figure 9 as L. According to the Lee company website, the volumetric flow rate for a gas can be determined using the following equations:[13]

$$Q = \frac{K f_T P_1}{L} \tag{15}$$

$$Q = \frac{2K f_T \sqrt{P_1(P_1 - P_2)}}{L} \tag{16}$$

$$f_T = \sqrt{\frac{294.3}{T(K) + 273.15}} \tag{17}$$

K is a units constant for a particular gas, f_T is a temperature correction factor shown in equation 17 for a gas at $70°F$ in Kelvin, P_1 denotes the pressure flowing into the valve which in this scenario is the stagnation pressure of the plenum, and P_2 denotes the pressure flowing out of the valve. One will notice that equation 15 does not rely on the downstream pressure at all, because it is the scenario in which the flow is choked through the valve because the pressure ratio meets the following condition:

$$\frac{P_1}{P_2} \geq 1.9 \tag{18}$$

As it turns out, the pressure coming out of the valve is always low enough that flow is choked so equation 15 is used for calculating the mass flow rate. Equation 16 would need to be checked against as well if the valve was being modeled as emptying into another tank like the plenum or into an atmosphere. However, since the valve modeling in question is for flowing propellant from the plenum into a vacuum, the second equation is ignored. Multiplying Q by the density of R-236fa and accounting for units, the mass flow rate is solved for the thruster. This mass flow rate expression and equation 14 are used with Matlab's ode45 to solve for the plenum states. These states, isentropic flow equations, and the known valve efficiency of η_{valve} are used to then calculate the performance characteristics of the thruster.

The time history of pressure, temperature, and mass in the plenum is post-processed to find the performance of the thruster. However, since the valve does result in pressure losses, the states post valve need to be used in the insentropic flow equations for determining performance. The post valve pressure and temperatures are found using:

$$P_p = P_0 \eta_{valve} \tag{19}$$

$$T_p = T_0 (\eta_{valve})^{1 - \frac{1}{\gamma}} \tag{20}$$

Where γ is the specific heat ratio of R-236fa. These intermediate pressures and temperatures are used to then solve for the flow conditions at the exit of the nozzle. The exit Mach number is determined by the nozzle area ratio and specific heat value of the propellant, and is used to determine the exit pressure P_e and exit temperature T_e. Exit temperature is used to determine the exit speed of sound, which is then used with

American Institute of Aeronautics and Astronautics

the exit Mach number to determine the exit velocity of the flow u_e. Denoting the exit area of the nozzle as A_e, thrust and specific impulse for the thruster model are then found using the following equations:

$$\tau = \dot{m}u_e + P_eA_e \tag{21}$$

$$I_{sp} = \frac{\tau}{\dot{m}g_0} \tag{22}$$

Starting with an analysis of a cold gas thruster firing at room temperature (25°C) and the plenum at 90 percent of the saturated liquid-vapor pressure of the main tank, the thruster model was evaluated for firing a single nozzle at a time.
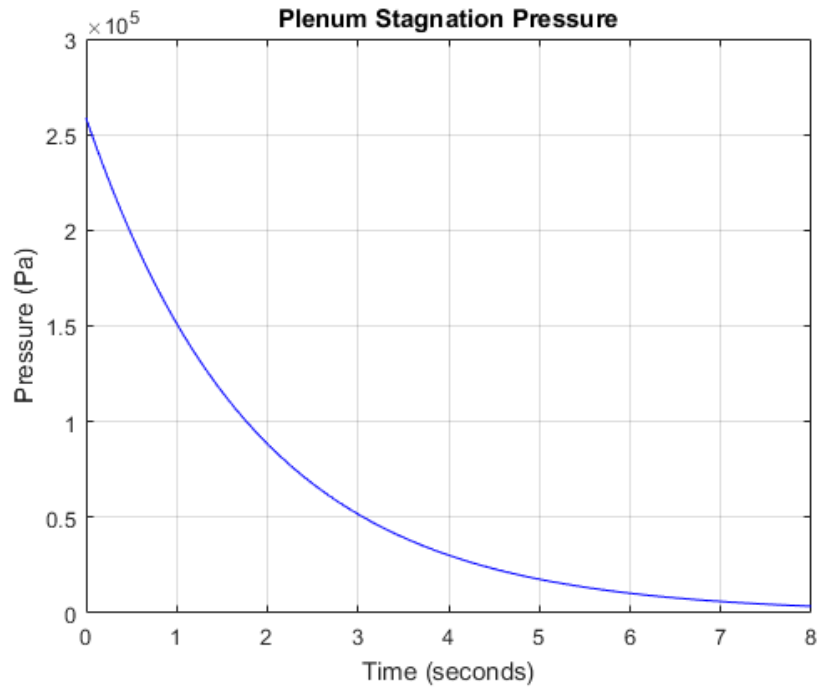
Figure 10. Thruster Simulated Plenum Pressure Profile for One Nozzle Fire

American Institute of Aeronautics and Astronautics
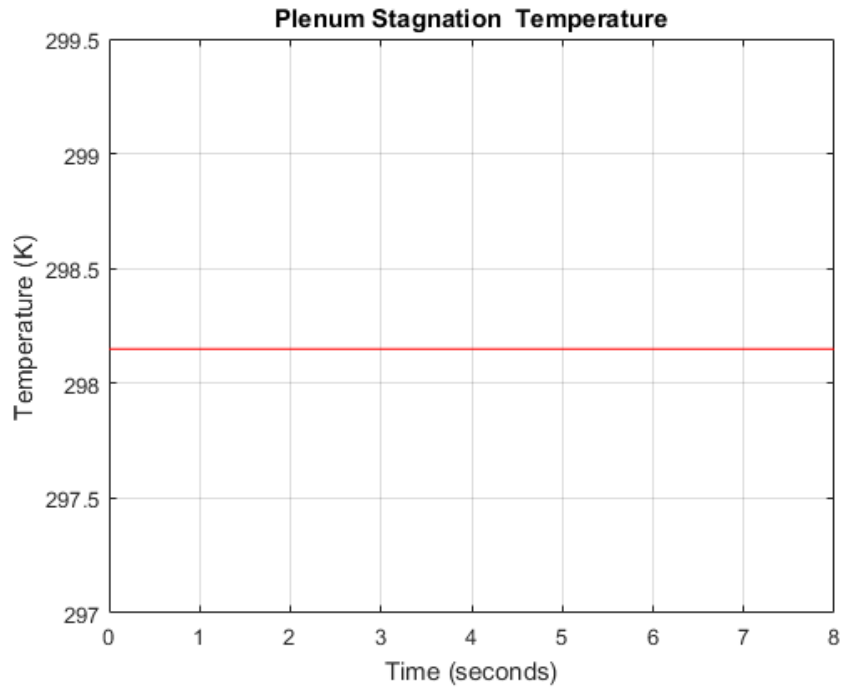
Figure 11. Thruster Simulated Plenum Temperature Profile for One Nozzle Fire
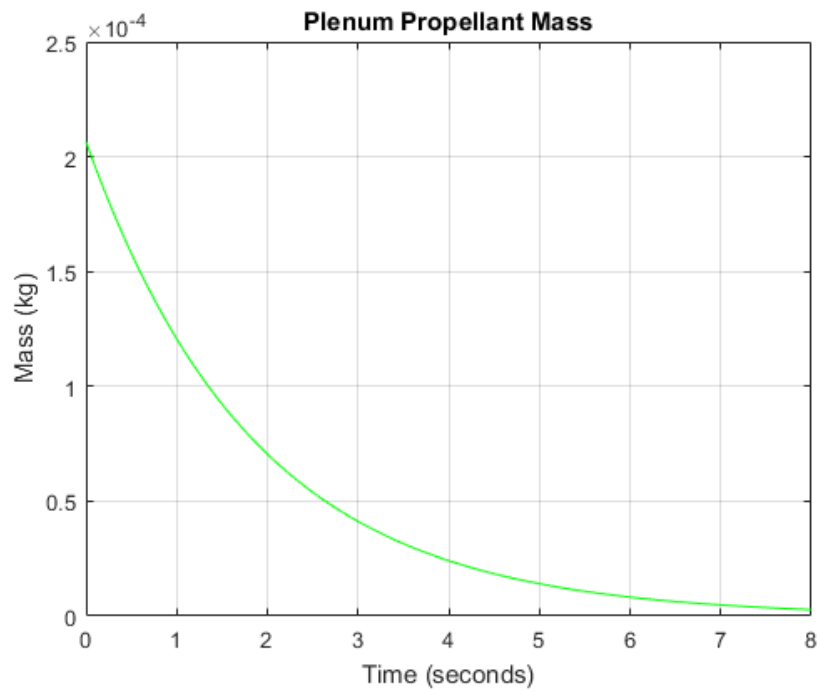
Figure 12. Thruster Simulated Plenum Mass Profile for One Nozzle Fire

American Institute of Aeronautics and Astronautics
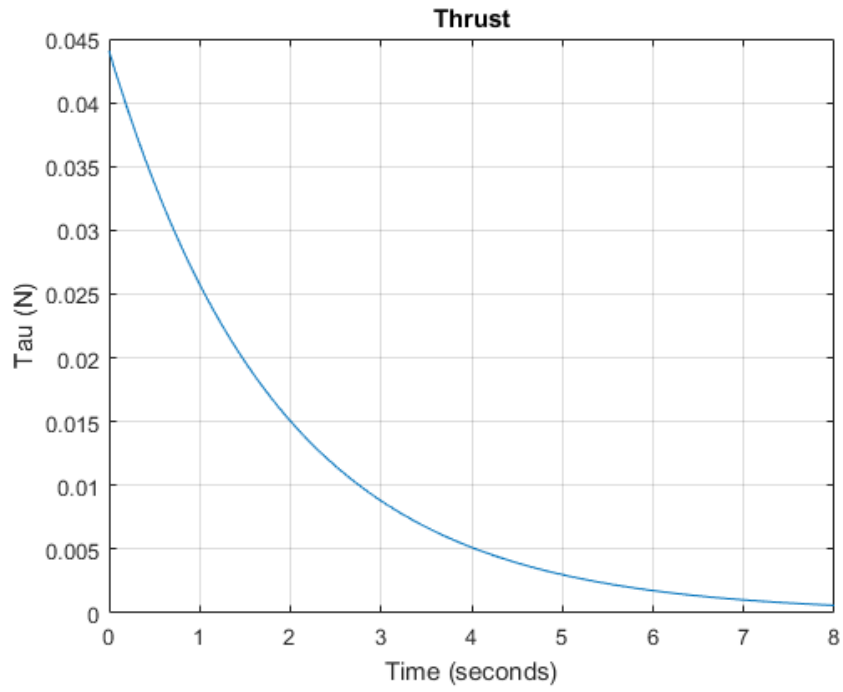
Figure 13. Thruster Simulated Thrust Profile for One Nozzle Fire
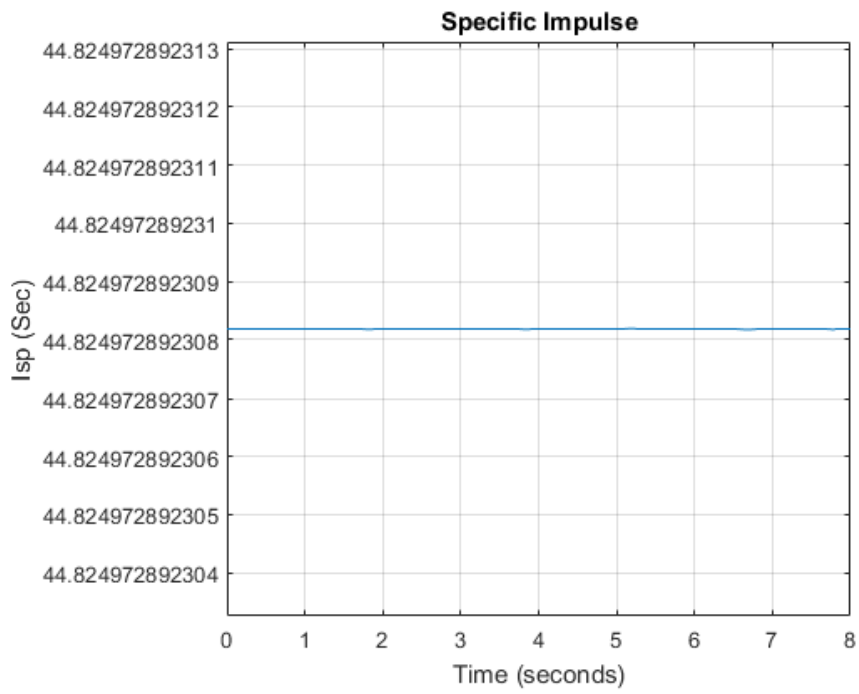
Figure 14. Thruster Simulated Specific Impulse Profile for One Nozzle Fire

American Institute of Aeronautics and Astronautics

These results are promising as they are in-family with observations from multiple data campaigns of the BioSentinel thruster.[5] Specific impulse is constant as predicted in theory and observed in test campaigns, and the magnitude of thrust appears to be in-line with previous observations. However, the length of sustained thrust appears to be a bit longer than expected, as observations show that average thrust drops off very quickly within a second of firing a full plenum to around the 20 mN line.[5] This error is possibly due to not modeling the flow restriction of the 5-micron filter used on the BioSentinel thruster.

To test the controller developed in the previous section, a Simulink simulation of the dynamics, controller, and thruster model are used to test the ability of the controller to respond to angular momentum commands. Since the developed controller depends on feedback about the angular momentum state of the satellite as well as pressure in the plenum, further models need to be constructed around each of these parameters.

The angular momentum and hence angular velocity of the satellite is the result of the integrated angular accelerations from an initial condition. These accelerations are modeled according to equation 5. As shown by the previous work, pressure in the plenum and mass flow rate are complicated quantities based on nonlinear equations. However, Figure 10 appears to show pressure taking on the shape of an exponential decay of the form:

$$P(t) = P_0 e^{-\alpha t} \tag{23}$$

Where α is a time constant modeling the rate at which the plenum pressure decays. This model is also very convenient because it means that the rate of pressure loss $\dot{P}(t)$ can be modeled as:

$$\dot{P}(t) = -\alpha P(t) \tag{24}$$

However, it is necessary to find this time constant. Using the time series of generated pressures from ode45 and the initial pressure used for the simulation with the following linearized model:
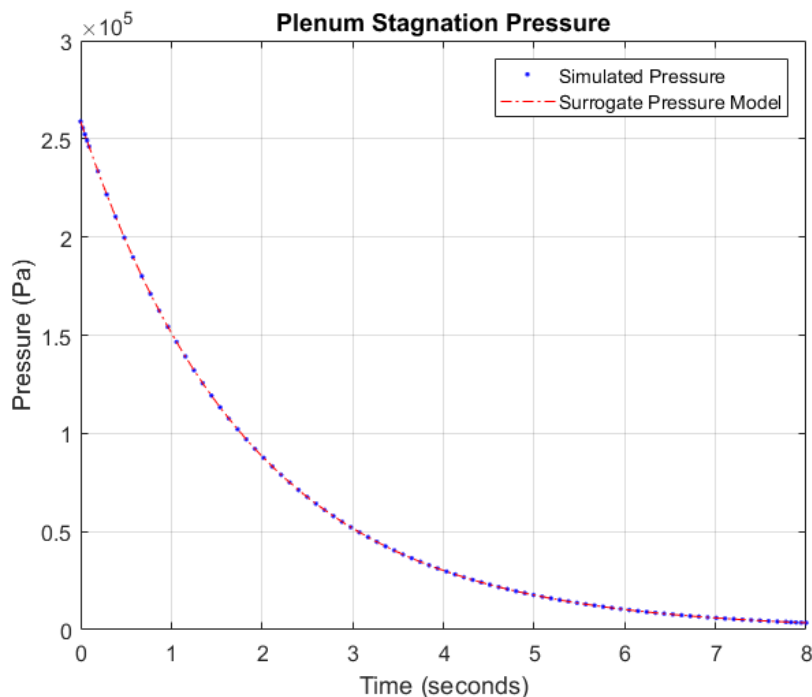
$$ln(P(t)) = ln(P_0) - \alpha t \tag{25}$$

Figure 15. Dynamically Modeled and Surrogate Modeled Plenum Stagnation Pressure.

A batch estimator was used to fit the data to find a best-fit α value. For the particular simulation of the thruster run, this surrogate model plotted against the outputted ode45 results look very identical as shown

American Institute of Aeronautics and Astronautics

in Figure 15, hence the model was accepted. From rocket propulsion theory, it is expected that pressure and thrust should have some positively correlated relationship.
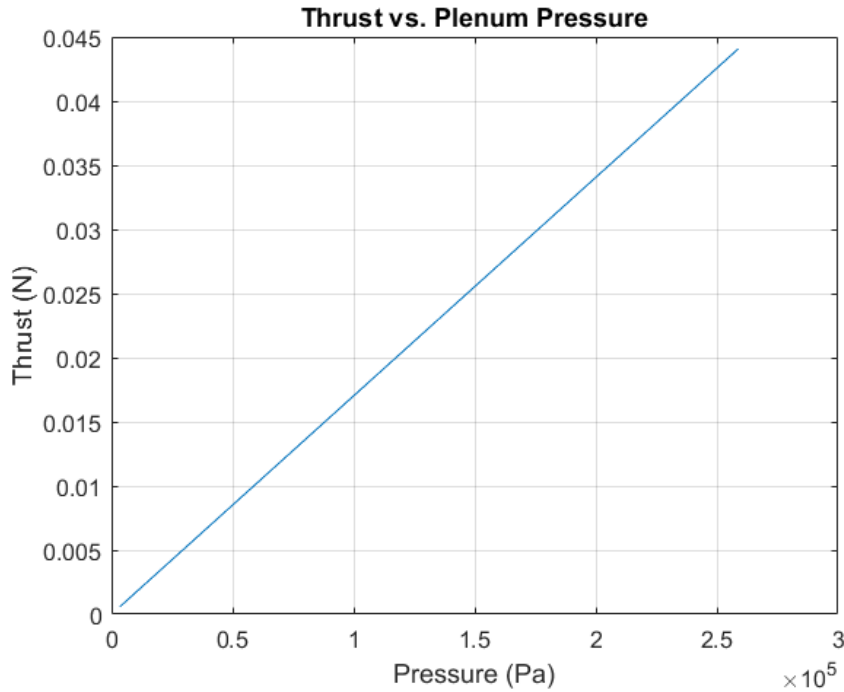

Figure 16. Thruster Simulated Thrust vs. Simulated Plenum Pressure

Figure 16 shows that there is a linear relationship for the developed thruster simulation. Thus, for the Simulink simulation the output thrust shall be modeled in the following way:

$$\tau(t) = \lambda P(t) \tag{26}$$

Where λ is a linear coefficient relating pressure to thrust in units of Newtons per Pascal.

The final determination is how to model the mass flow rate being dependent on plenum pressure. Looking at a similar graph for mass flow rate and plenum pressure rate, one would assume that the linear relationship is through the rearranging of equation 14. Equation 14 would imply that the only things composing the slope of the trendline in Figure 17 are the gas constant, temperature, and volume of the plenum. For whatever reason, this turns out to be not totally true. A constant multiplier offset was found in the slope values when comparing surrogate models to actual data output. The extra multiplier term k_1 is found as the following:

$$\dot{m} = \frac{\dot{P}(t)V_{plenum}}{k_1 R T_{plenum}} \tag{27}$$

This is what is modeled in the Simulink simulation for the SPUDnik system. This is an area of future work to determine why this is present, it most likely is a simple be a math mistake made while modeling, or it may be of some other unknown origin. Either way, it achieves accuracy with the surrogate model for determining mass flow rate based on pressure change.
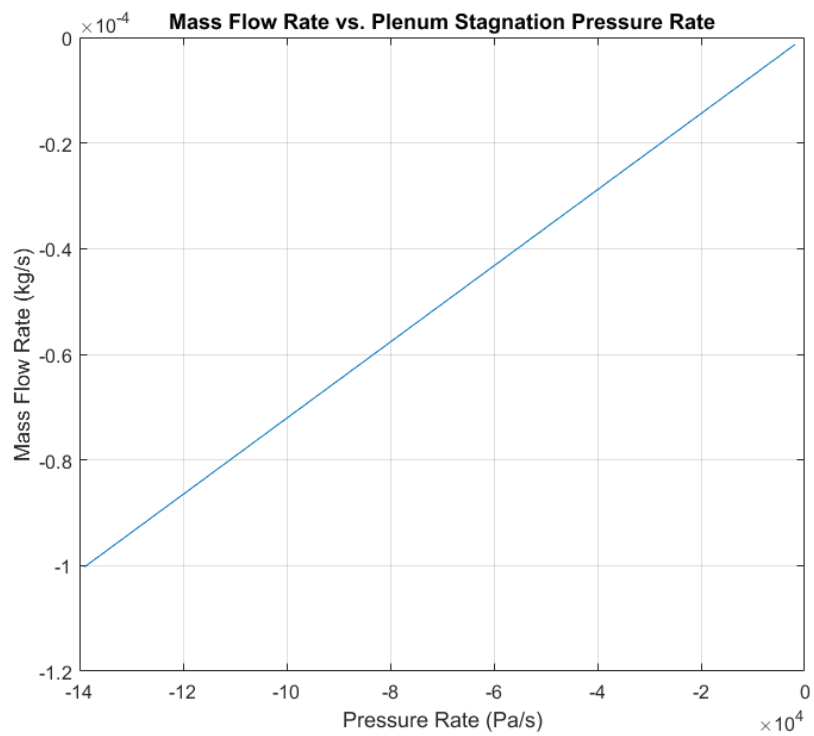
American Institute of Aeronautics and Astronautics

Figure 17. Thruster Simulated Mass Flow Rate vs. Plenum Pressure Rate

C. Satellite Simulation and Results

Using the dynamics, control scheme, and thruster plant models described in the previous section, a Simulink model was constructed to test the ability of the thruster controller. The improvement this controller presents is commanding the thruster to a desired angular momentum state by determining the time to open valves autonomously rather than receiving timed commands. This controller also manages the plenum pressure more closely ensuring repeatability of performance between nozzle firings.
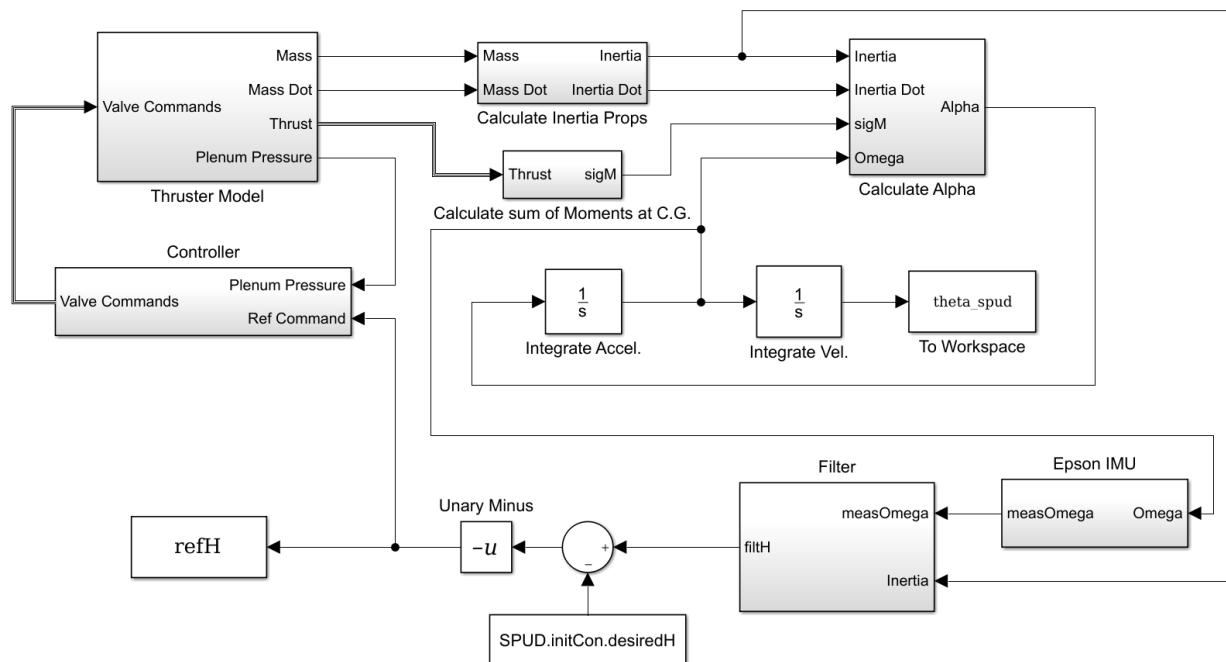
Figure 18. Simulink Thruster Closed-Loop Simu lation

This thruster simulation main Simulink diagram is shown in Figure 18. There are blocks shown for an inertial measurement unit and filter, however, due to time constraints these were not fully implemented in the model. Instead, the results presented are assuming perfect knowledge of the thruster angular momentum state.

The thruster controller implemented in Simulink is shown in Figure 19. This controller as mentioned previously checks the pressure in the plenum before deciding what valves need to fire if the norm of the reference angular momentum value is greater than the necessary tolerance. This controller as it stands is made for a SPUDnik unit of up to eight nozzles thereby providing full six degree of freedom control, but can take arbitrary positive integer number nozzles less than eight. The controller outputs a vector of binary 1's and 0's indicating what valves need to open on the thruster plant.

The thruster plant in Simulink is shown by Figure 20. Valve firing commands are fed into each of the necessary plant outputs, where each subsystem calculates its quantities. Everything as described previously works based on the values of plenum pressure and the rate of pressure change in the plenum. The plant currently does not take into account the fact that valves have a finite opening and closing time. Future work would dictate adding this feature in.

Table 2. Worst Case Scenario Tip-Off Rates

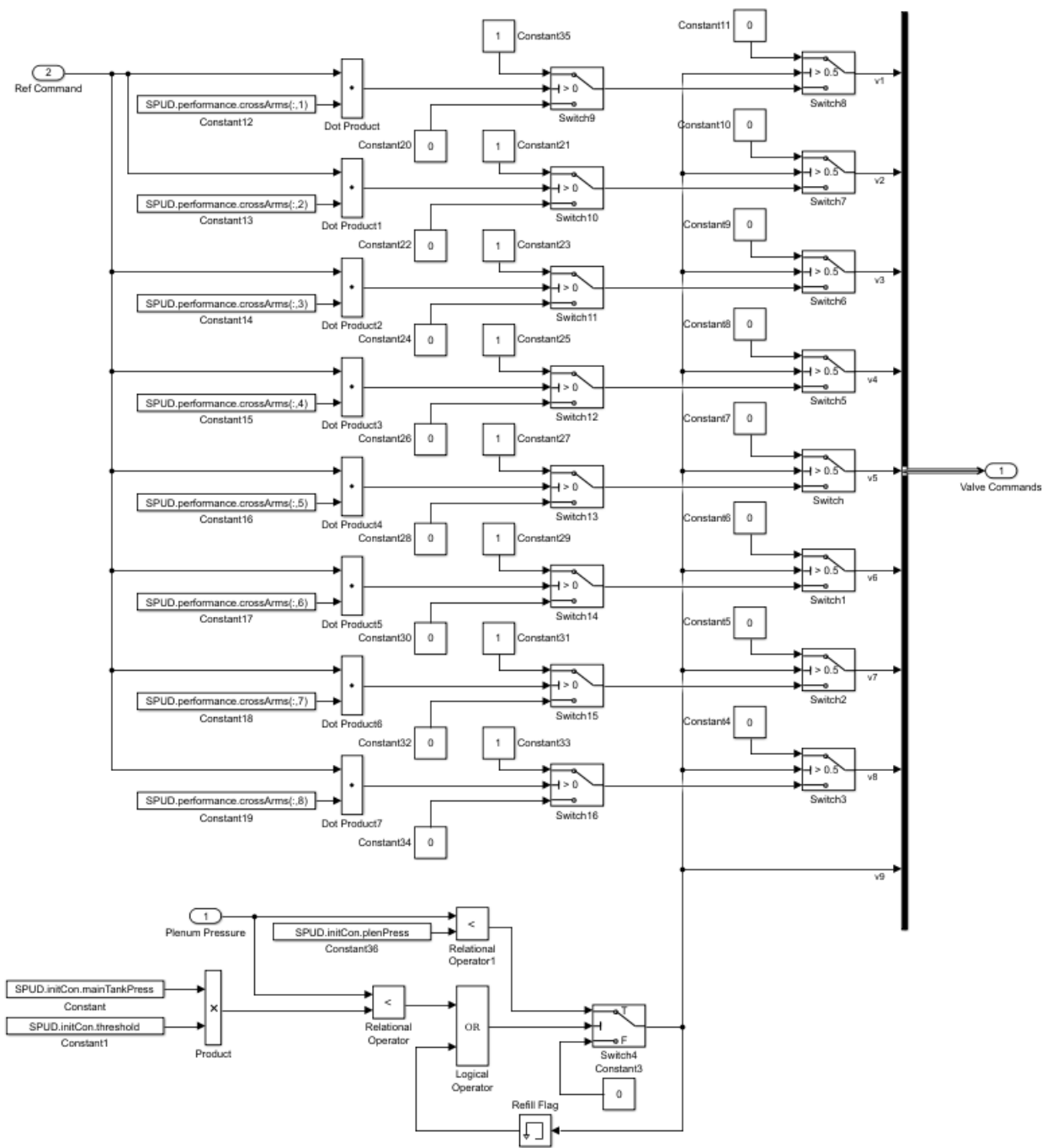| $\omega_x(°/s)$	$\omega_y(°/s)$	$\omega_z(°/s)$
12.0	-8.0	-10.5

American Institute of Aeronautics and Astronautics

Figure 19. Simulink Thruster Controller Implementation

In order to run a simulation, a few initial conditions are required. To demonstrate the usefulness of this controller, the de-spinning of a freshly deployed CubeSat is examined. Using values in Table 2 for worst case initial tip-off rates from a canister,[14] the performance of the controller is tested. The plenum threshold values are 80 and 95 percent of the main tank pressure, the gas temperature is assumed to be 25°C, and the mass of the CubeSat and propellant is that of SPUDnik. The spacecraft is spinning and the desired state is that the spacecraft is no longer spinning so it can orient itself and begin checkouts.

Figures 21, 22, and 23 best demonstrate the performance of the new closed loop controller. The controller
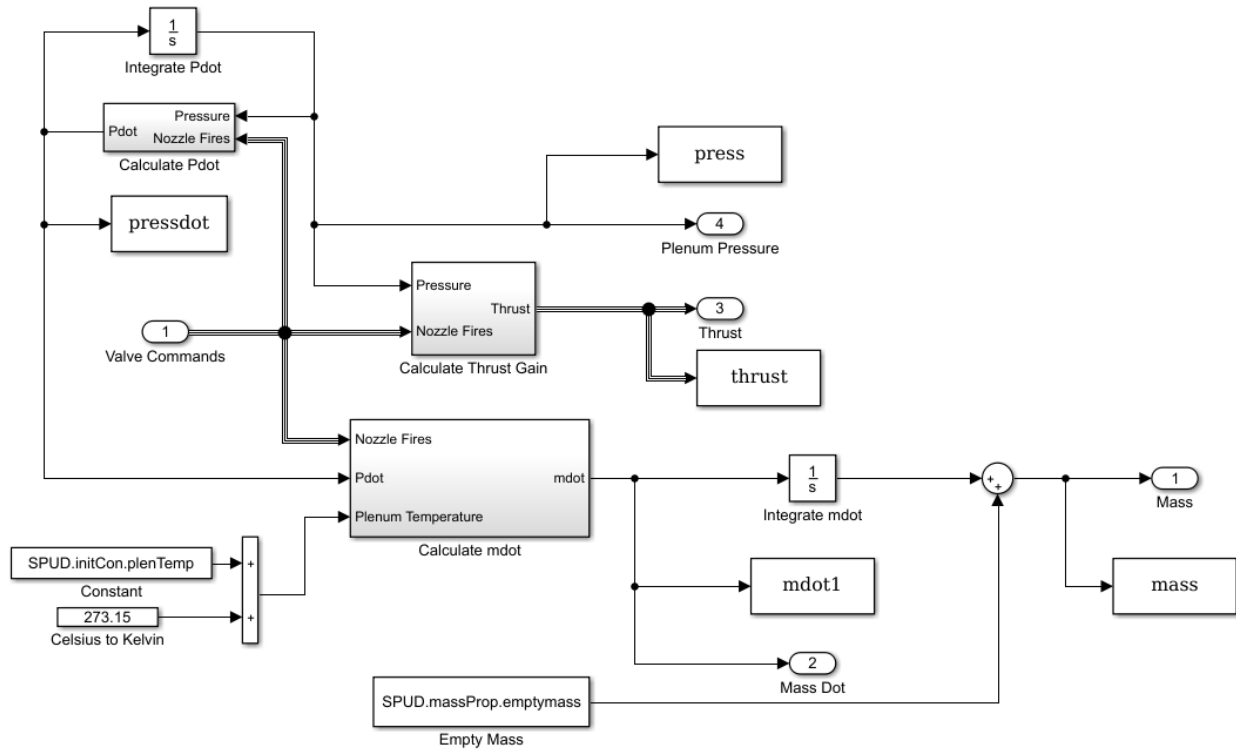
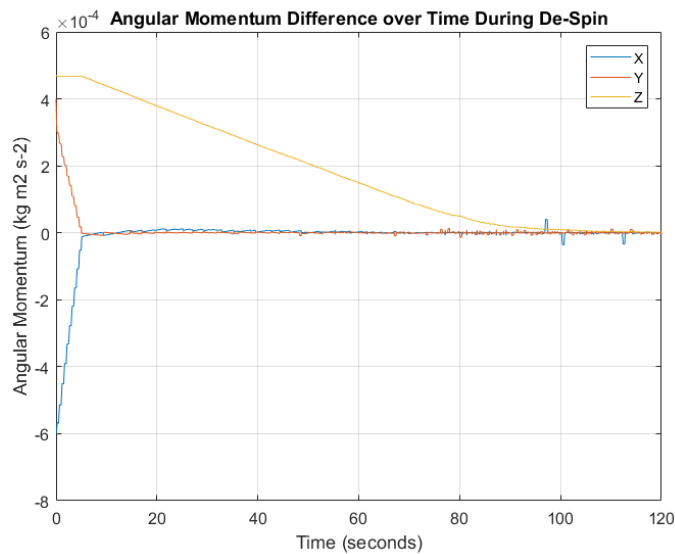Figure 20. Simulink Thruster Plant

Figure 21. Simulated Angular Momentum Difference

does indeed converge to the desired state, albeit quickly in some axes and slower in the Z axis. This is due to the orientation of nozzles, and that nozzles have the least control authority in the Z axis. Figure 24 shows the thruster controller working in more detail. The angular momentum difference vector follows a stepping motion in each axis since the thruster is refilling during periods of no angular momentum change, and then stepping down in angular momentum difference while firing.

This de-spin maneuver ultimately eats approximately 15.6 grams of fuel. This is not completely desirable
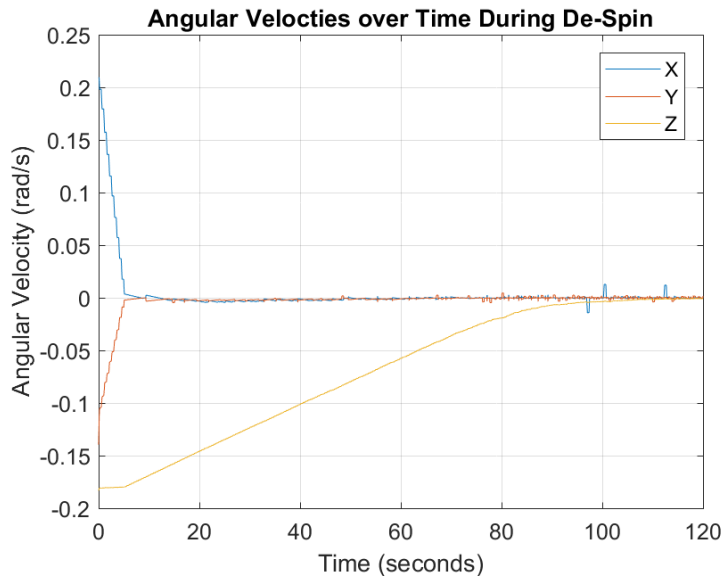
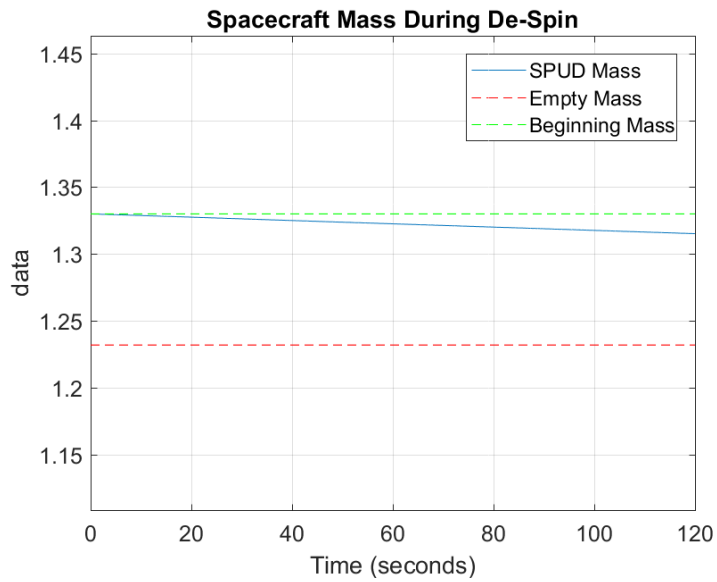**Figure 22. Simullated Angular Velocity Profile**

Figure 23. Simulated Spacecraft Mass

as this represents about 16 percent of the available fuel. However, if this thruster is used in conjunction with reaction wheels on an actual deep space mission, this may be acceptable since these kind of de-saturation maneuvers would hopefully only occur a few times well within the propellant load of the spacecraft.
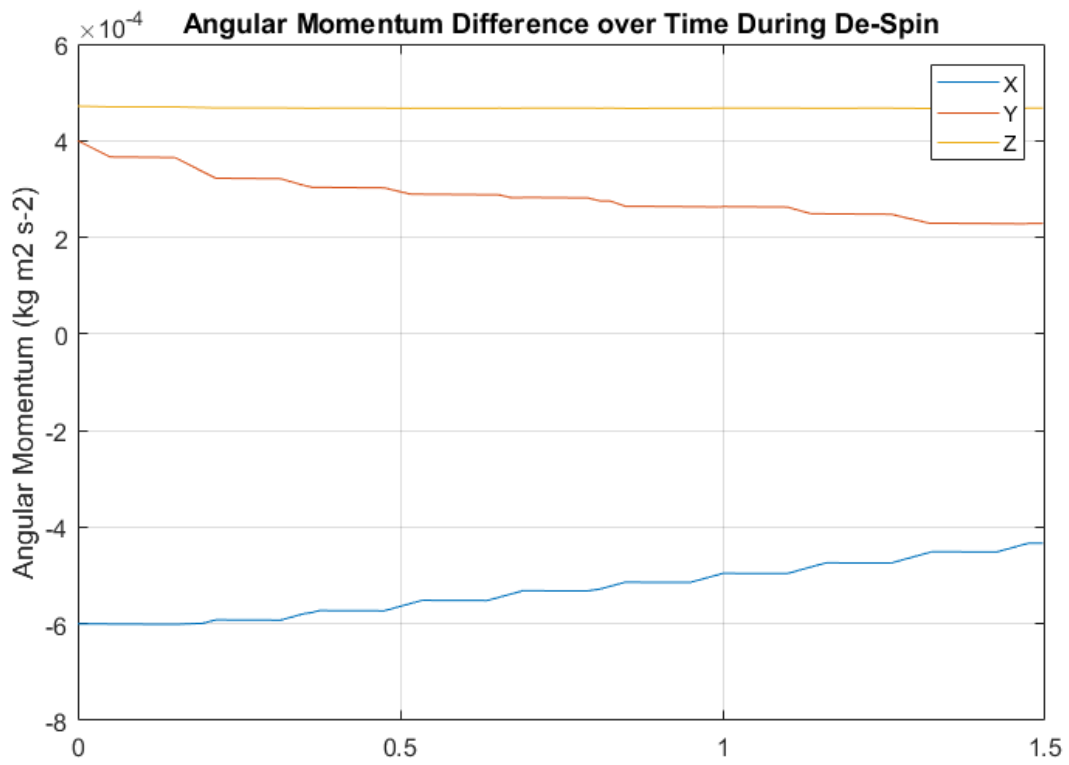
Figure 24. SPUDnik Step Firing

IV. Implementing Radiation Tolerant Electronics

To enable deep space exploration using something like a 1U additively manufactured satellite, one of the largest hurdles to overcome is that of the intense radiation environment in space. Things like single event upsets and total ionizing dosage affect electronics leading to unwanted bit flips, uncommanded events, and up to total failure of the electronics altogether. To mitigate these effects, work has been done investigating the use of a radiation tolerant microcontroller.

The microprocessor identified as a possible replacement for current thruster electronics is the Microchip ATmegaS128 (AMS128). This processor offers onboard memory storage, eight analog-to-digital (ADC) ports for reading in sensor data, and operates nominally around 3.3V[15] making it a strong candidate for a CubeSat Attitude Determination and Control processor.
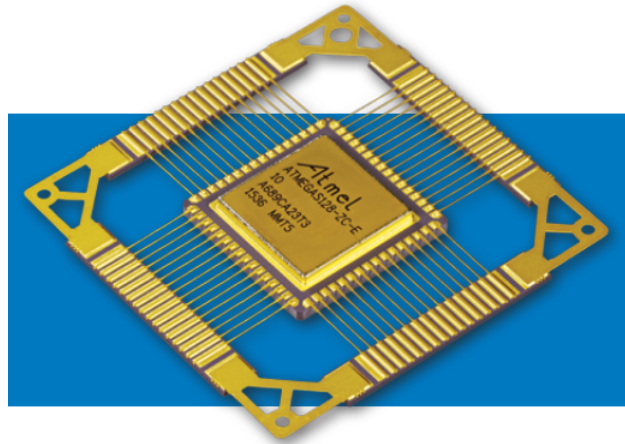

Figure 25. ATmegaS128 Microcontroller

One of the immediate drawbacks of using the AMS128 is the fact four of the JTAG lines are shared with ADC lines rendering half of the ADCs useless. Microcontroller JTAG lines are used for debugging prototype boards while the chip is powered on and connected to appropriate circuitry. This allows the engineer to develop software and test it line by line on actual hardware, which is especially great during development phases. Normally these lines are not used once a board design is finalized and robust enough that it enters into mass production. However, CubeSats designs and most satellite designs are always the first of their kind to be built and LRG thrusters are no different. The ability to rewrite and test software at all times is highly desired because if some unforeseen event happens, the unlucky engineer will have the pleasure of de-integrating their thruster and trying to fix the board or make a new board altogether.

The lack of ADCs is not the end of the world as current thruster designs only need up to four ADCs anyway since there are only four analog sensors. However, if more pressure/temperature sensors are desired for the thruster, then the design engineer will have to find a new route. There are workarounds, but they require external ADCs to be added onto the board which equals a larger board footprint which may end up eating into tank volume if it is too large.

The next issue encountered is actually procuring an AMS128. While vendors exist that sell the microcontroller in question, being a university lab is not exactly the biggest motivator for vendors to sell small amounts of low production volume items. That being said, the AMS128 has the distinction that it is almost a drop-in replacement in terms of software, pin assignments, and printed circuit board (PCB) footprint as its non-radiation tolerant cousin, the ATmega128. This means that a board can be developed around the non-radiation tolerant microcontroller, tested, and in theory the AMS128 should be swapped in its place once finally procured.

To evaluate the performance of the 128 chips, a PCB containing all of the traditional LRG thruster electronics was designed and a layout created as shown in Figure 26. The board was manufactured as
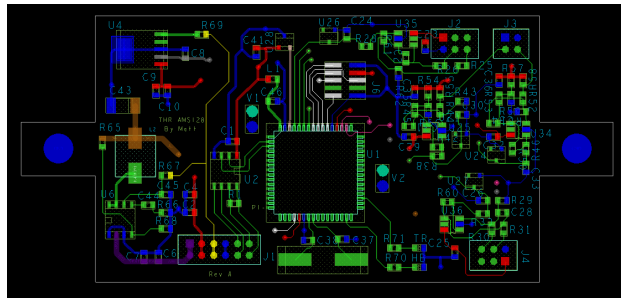
American Institute of Aeronautics and Astronautics
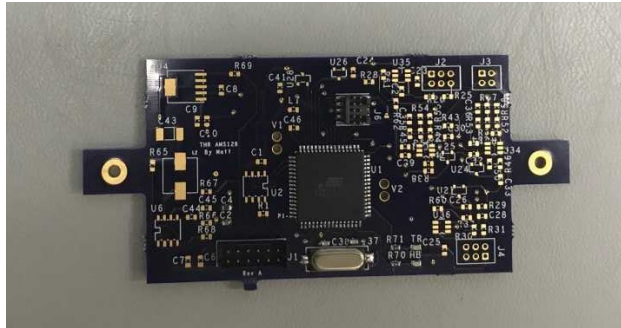
Figure 26. Early Layout Design of Board

Figure 27. Board During Manufacturing

seen and completed. Basic continuity checks were completed and rudimentary software was written to test communications capabilities over the JTAG lines. However, due to time constraints the implementation of the controller designed in Simulink and all other supporting software was not completed leaving this section as a major future work opportunity.

V. Conclusion

Various aspects of enabling deep space maneuverable CubeSats were examined in this paper. The design of a scaled down version of SPUD known as SPUDnik was designed and simulated in Simulink with a new controller design than previously used on other LRG thrusters. Additively manufactured satellites with propulsion systems printed into the main structure again proved to be more volumetrically efficient than SLA printed thrusters. The metal printed thruster-satellite hybrid presents an improvement in performance capabilities over the traditional SLA printed thrusters due to the volumetric efficiency of combining satellite structure with propulsion system. In a smaller volume allocation, SPUDnik has more nozzles and nearly matches propellant capacity to that of the Bevo-2 thruster which is the closest in size to the SPUDnik case study.

In the simulation, while the satellite achieved a successful de-spin maneuver using worst case scenario tip-off rates, the 16 percent of total propellant used in conjunction with no additional room for reaction wheels inside of SPUDnik means that the spacecraft most likely would have a very short life span. Because of this, it is necessary to either resize the propellant storage on the satellite to allow for the addition of reaction wheels to store momentum, or increase the size of the spacecraft to 1.5U and examine results there. However, that being said the 1U SPUDnik would be the possible cheapest option for the testing of additively manufactured satellite-thruster systems and new control schemes.

The last part of this work was to design an electronics board for LRG thrusters around a new radiation tolerant microcontroller known as the ATmegaS128. While the board was designed, built, and elementarily tested, the control scheme developed in Simulink was not implemented. In fact, the programming of the board and subsequent testing did not occur due to time constraints. While the AMS128 does not have a

American Institute of Aeronautics and Astronautics

large number of ADC ports and has a large footprint on the board, the radiation tolerant aspect is too attractive to pass up and should be continually explored past this paper.

VI.   Future Considerations

The first thing on the agenda for future work is the finishing of evaluation for the ATmegaS128 processor. Deep space satellites most likely will fail in large numbers if the electronics onboard are not capable of surviving radiation. One of the hurdles in evaluating the AMS128 was actually procuring an AMS128. As they are aerospace special, it is necessary to build good working relationships with suppliers to acquire one. However, in the meantime use of the non-radiation tolerant ATmega128 is acceptable since the AMS128 acts as a drop-in replacement even in footprint.

This work introduced the highest fidelity simulation of a cold gas thruster system in LRG to date. Continued improvement to this simulation as well as integration with future satellite mission day in the life tests would be highly beneficial to the lab. This simulation also allows for possibly settling the plenum sizing debate that has occurred over a number of years. Testing the simulation against actual hardware measurements would act as a key way to help increase fidelity as errors in the model are found and corrected. Another thing that was not done in this paper was the creation of a filter. The pressure, temperature, and eventually inertial measurement unit will have noise in the measurements they present to the thruster. Since the controller works on binary threshold states, it is important to make sure that signals are as clean as possible so that no erroneous valve commands are made.

Future work for the design of SPUDnik includes looking at printing just the thruster portion of the satellite. The CAD for SPUDnik was made under the assumption that eight nozzles would be used with four of them using the railing for piping. However, those four nozzles were cut due to space limitations and thus the rest of the satellite CAD was left as part of the printed structure. Due to the cost, and high risk of sabotaging the entire satellite structure with a bad helicoil install, it would be beneficial to redesign SPUDnik as just a metal printed thruster that has the CubeSat rails on it. This metal printed standalone thruster would would serve as an endcap of sorts for the satellite.

This paper only explored the capabilities of the 1U SPUD design, whereas other sizes of CubeSat are possible. The tools developed for this paper are hopefully modular enough so that future researchers may easily explore the capabilities of other standard CubeSat sizes using the concept of combined thruster and satellite structure. Designing reference missions and exploring capabilities is invaluable to satellite mission designers who require propulsion for their satellites, especially as CubeSats march more frequently into interplanetary space.

American Institute of Aeronautics and Astronautics

References

[1] J. Davis. Here's what you need to know about the electron rocket, 2017.

[2] S. Arestie, E. Glenn Lightsey, and B. Hudson. Development of a modular, cold gas propulsion system for small satellite applications. *Journal of Small Satellites*, 1(2):63–74, 2012.

[3] Gunter's Space Page. Bevo 2, 2019.

[4] T. Stevenson. Design and testing of a 3d printed propulsion system for small satellites. Master's thesis, Universtiy of Texas at Austin, May 2015.

[5] E. Glenn Lightsey, T. Stevenson, and Sorgenfrei M. Development and testing of a 3-d-printed cold gas thruster for an interplanetary cubesat. *Proceedings of the IEEE*, 106(3):388, 2018.

[6] T. Imken. Design and characterization of a printed spacecraft cold gas thruster for attitude control. Master's thesis, University of Texas at Austin, May 2014.

[7] T. Stevenson. *Development of Multi-Functional Structures for Small Satellites*. PhD thesis, Georgia Institute of Technology, December 2018.

[8] VACCO. Jpl marco - micro cubesat propulsion system, 2018.

[9] Interpro Models. 3d printing materials, 2019.

[10] DuPont Fluoroproducts. Hfc-236fa clean agent. properties, uses, storage, and handling, 2012.

[11] S. et al. Lee. *CubeSat Design Specification (CDS)*. The CubeSat Program, Cal Poly SLO, rev. 13 edition, February 2014.

[12] J. S. LILLEY and J. D. HOFFMAN. Performance analysis of scarfed nozzles. *Journal of Spacecraft and Rockets*, 23(1):55–62, 1986.

[13] The Lee Co. How to calculate flow resistance for gases, May 2019.

[14] F. Azure, R. Hevner, and W. Holemans. Lessons learned measuring 3u and 6u payload rotation and velocity when dispensed in reduced gravity environment. Slide show, Planetary Systems Corporation, April 2015.

[15] Microchip. *Rad-Tol 8-bit AVR Microcontroller, 3.3V, 8 MHz with 128 KB Flash, 4KB EEPROM, 4KB SRAM, 10-bit ADC, TWI, RTC, 16-bit PWM, USART, SPI and 16-bit Timer/Counter*. Microchip Technology, 2017.